Distribution of Carbon Nanotube Sizes from Adsorption Measurements and Computer Simulation

Piotr Kowalczyk,*,†,‡ Robert Hołyst,‡ Hideki Tanaka,† and Katsumi Kaneko†

Department of Chemistry, Faculty of Science, Chiba University, 1-3 Yayoi, Chiba, 263, Japan, and Department III, Institute of Physical Chemistry, Polish Academy of Science, Kasprzaka Street 44/52, 01-224 Warsaw, Poland

Received: April 21, 2005; In Final Form: June 6, 2005

The method for the evaluation of the distribution of carbon nanotube sizes from the static adsorption measurements and computer simulation of nitrogen at 77 K is developed. We obtain the condensation/evaporation pressure as a function of pore size of a cylindrical carbon tube using Gauge Cell Monte Carlo Simulation (Gauge Cell MC). To obtain the analytical form of the relationships mentioned above we use Derjaguin−Broekhoff−deBoer theory. Finally, the pore size distribution (PSD) of the single-walled carbon nanohorns (SWNHs) is determined from a single nitrogen adsorption isotherm measured at 77 K. We neglect the conical part of an isolated SWNH tube and assume a structureless wall of a carbon nanotube. We find that the distribution of SWNH sizes is broad (internal pore radii varied in the range 1.0−3.6 nm with the maximum at 1.3 nm). Our method can be used for the determination of the pore size distribution of the other tubular carbon materials, like, for example, multiwalled or double-walled carbon nanotubes. Besides the applicable aspect of the current work the deep insight into the problem of capillary condensation/evaporation in confined carbon cylindrical geometry is presented. As a result, the critical pore radius in structureless single-walled carbon tubes is determined as being equal to three nitrogen collision diameters. Below that size the adsorption−desorption isotherm is reversible (i.e., supercritical in nature). We show that the classical static adsorption measurements combined with the proper modeling of the capillary condensation/evaporation phenomena is a powerful method that can be applied for the determination of the distribution of nanotube sizes.

1. Introduction

Gas adsorption, especially adsorption of nitrogen and argon at the boiling point temperature, has been an important tool for characterization of surface and structural properties of nanoporous solids such as adsorbents, catalysts, and other related materials.[1,2,3] Consequently, many theoretical approaches used for the interpretation of the gas adsorption measurements have been developed so far.[4] Unfortunately, many of those methods produce inconsistent and unreliable results.[5,6] So, the most important and timely problem is an experimental verification of the aforementioned methods.

In the case of regular nonporous silica type materials, such as MCM-41, FSM-16, FDU-2, SBA-15, etc., the prediction of the structural properties obtained from the classical gas adsorption measurements can be easily compared with those determined from the other experimental methods (i.e., XRD, high-resolution transmission electron microscopic observation (HR-TEM), etc.).[6,7] Those high-purity materials have ordered pore structures and fixed pore shape and size.

On the other hand, a great number of carbonaceous materials, mostly activated carbons, are characterized by broad distribution of pore sizes. Therefore, the direct estimation of the structural heterogeneity by XRD or other independent methods is a very difficult problem.[8] These materials include the multiwalled carbon nanotube (MWCN),[9] double-walled carbon nanotubes (DWCN),[10] and single-walled carbon nanotubes (SWCN).[11−14] Similarly to fullerene, both SWCN and MWCN are synthesized by the electric arc discharge or laser ablation of a carbon rod. Consequently, they contain some amount of impurities (i.e., Fe, Ni, Co, or their mixtures).[9] DWCN is a high-purity carbon material prepared with chemical-vapor deposition.[10] They consist of two concentric graphene cylinders, a structure that is intermediate between SWCN and MWCN. As mentioned by Endo et al.[10] DWCNs are a very promising kind of carbonaceous material due to their unique mechanical properties, thermal conductivity, structural stability, or gas storage possibility.[10]

Recently, Iijima et al. synthesized a single-walled carbon nanohorn (SWNH)[15] of purity >95%. Such high purity of SWNH is due to synthesis conditions, i.e., CO_2 laser ablation of graphite under argon gas flow at 760 Torr without metallic catalysis. SWNHs form "a *dahlia* flowerlike structured assembly" of 80 nm size (see Figure 1).[15,16] The X-ray diffraction study showed that the interhorn−wall distance is 0.4 nm, being greater than the interlayer spacing of graphite (0.335 nm).[17] The average diameter of a single tube in this assembly and length is estimated from HR-TEM as 2−3 and 40−60 nm, respectively.[16,17] *However, the average diameter obtained from HR-TEM is not sufficient to determine the broad distribution of pore sizes*.

Such distribution can be obtained from adsorption data as shown in this paper. From the simple geometric considerations (notice that SWNH has a closed horn-shaped tip with a cone

* To whom correspondence should be addressed. E-mail: kowal@kora.ichf.edu.pl.
† Chiba University.
‡ Polish Academy of Science.

10.1021/jp0520749 CCC: $30.25
Published on Web 07/08/2005

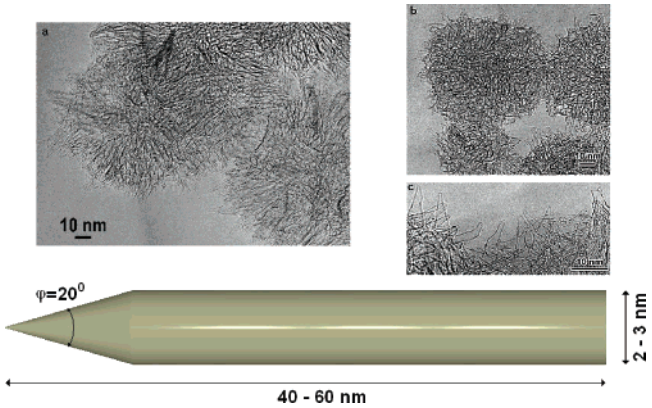

Figure 1. High-resolution TEM images of "a *dahlia* flowerlike structured assembly" of SWNHs. The bottom part of the figure presents an isolated SWNH model.

angle of about 20°)[15−17] it is clear that the thermodynamic properties (i.e., absolute and excess value of adsorption) of SWNHs predominantly depend on their tubular part, whereas the adsorption in the conical cap can be neglected.[18] Originally, in "a *dahlia* flowerlike structured assembly" the SWNHs are closed for the gas penetration, i.e., the adsorption can only take place on their external surface.[15,18] The controlled process of burning can open the carbon tubes.[16] It is obvious that burning creates the holes preferentially at conical caps characterized by the strongest reactivity. Furthermore, it is reasonable that the structures of closed and opened SWNHs are very similar except for the created holes.[19] As a result the internal porosity of SWHN particle and interstitial porosity of SWNH aggregates can be separately determined by nitrogen adsorption at 77 K.

In the current paper we develop a method that can be used for the evaluation of the distribution of nanotube sizes from the adsorption measurement of nitrogen at 77 K and computer simulations. The relationship between capillary condensation/evaporation pressures and a pore size is obtained from the Gauge Cell MC implemented with thermodynamic integration. To check the consistency of the Gauge Cell MC the standard Grand Canonical Monte Carlo (GCMC) method is used for the generation of the whole adsorption isotherm. Further, we adopt the recently improved Derjaguin−Broekhoff−deBoer theory (IDBdbB) to the case of capillary condensation/evaporation in carbon cylindrical tubes to obtain the analytical form of the relationships mentioned above.[6] Next, we construct the pore size distribution of SWNHs according to the classical concept of the integral equation[20] as well as the modified Dollimore−Heal[21] method. Finally, we compare the adsorption isotherms obtained in computer simulation to the experimental one. In this way we obtain the distribution of pore sizes. Another outcome of this work is a better understanding of the impact of the pore size on the shifting of the capillary condensation/evaporation point in carbon cylindrical tubes.

2. Theoretical Models

2.1. Gauge Cell Monte Carlo Simulation with Thermodynamic Integration. The Gauge Cell MC implemented with thermodynamic integration is very powerful method based on statistical thermodynamics background.[22,23] For a case of novel regular silica type materials, the relationship between the capillary condensation/evaporation versus pore size can be determined experimentally since the detailed pore structure (i.e., average pore size and pore arrangement) is well-known and defined.[5,6] Moreover, novel regular silica-type materials are characterized by relatively small structural heterogeneity, which leads to experimental sharp first-order transition, high purity, absence of connectivity effect, regular arrangement of pores, negligible adsorption on the external surface, and so on.[5,24] Consequently, a theoretical model of capillary condensation/evaporation phenomena in confined geometry can be developed and verified experimentally.[6,25] Next, the derived relationship combined with the generally accepted concept of the integral theory of adsorption or modified DH algorithm can be easily used for the determination of the distribution of pore sizes.

In a case of tubular carbon type materials the situation is much more complicated due to several factors. The simplifications of the real "*dahlia* flowerlike structured assembly" of the SWNHs are necessary since the detailed model of these materials is very difficult to establish. At first, the structure of these materials (i.e., pore shape and arrangement) is not well defined (see Figure 1). Besides this, the distribution of pore sizes of SWNHs and SWCNs are broad.[18] It is rather hard to imagine how to design "a *dahlia* flowerlike structured assembly" of the SWNHs consisting of internal tubes of well-defined radii. For these reasons the experimental relationship between the pore size and capillary condensation/evaporation pressure in carbon nanotubes has not been established so far.

As we mentioned above, the second reasonable approximation is neglecting the adsorption in the conical cap of individual SWNHs and simplification of the model of the solid−fluid interactions. We must underline that the establishment of the detailed structure of the conical cap in the individual single-walled carbon nanohorn is difficult to overcome in a rigorous fashion. The perfect conical cap has never been observed, rather it can be skewed, unsymmetrical, deformed, and pierced by holes (see Figure 1). Consequently, the rigorous atomistic model of the SWNHs cannot be establish. We can rather built a replica of the real systems introducing inevitable mathematical complexity. For example, we can derive an expression for the structureless solid−fluid interaction potential in a separated cylindrical or conical element. Unfortunately, when we connect these two elements we obtain unphysical oscillation in the solid−fluid potential on the boundary between them. We can use some functions to smooth out the solid−fluid potential on that boundary but these functions are artificial from a physical point of view. For this reason such approaches have not received attention in the scientific community. Obviously, if we model the single-walled carbon nanohorn as a structureless tube and atomic conical cap we observe the same artificial behavior. Neglecting the conical cup is reasonable due to simple mathematical considerations. Let us consider that the individual single-walled carbon nanohorn is composed of a cylindrical tube (length: l_1; diameter: D) and the perfect cone (length: l_2; diameter of the base: D) part. The volume ratio of the cone part to the total volume of the single-walled carbon nanohorn can be calculated by $l_2/(3l_1 + l_2)$ and as shown by Tanaka et al.[18] is smaller than 6%, when the D value is 2 nm, and the lengths are $l_2 \approx 6$ nm and $l_1 + l_2 = 40$ nm, respectively (these values should be reasonable from TEM observations, see Figure 1). In conclusion, it is reasonable to neglect the adsorption quantity in the conical cap and model the single-walled carbon nanohorn as a straight structureless carbon tube. The adsorption in a single-walled carbon nanohorn can occur both inside and outside the tube because of the single layer of carbon atoms. In the simplest form we can include this effect neglecting the presence of the carbon wall; however, it is only a simplification since the wall exists and lightly deforms the interactions between molecules inside and outside the carbon tube. It is worth pointing

out that including fluid−fluid interactions between molecules outside and inside the carbon tube is particularly important when we model the adsorption isotherm in the bundle of nanohorns and compare with experimental results. In our proposition we calculated, not measured, the isotherm inside the SWNHs. By a simple procedure presented in the refs 15, 16, 18, and 19 we can obtain the pure overall adsorbed quantity inside the single-walled carbon nanohorn. We believe that such a simplification does not drastically deform the obtained results; however, we are considering the further development of the presented methodology.

Here, we use the Gauge Cell MC combined with thermodynamic integration to obtain such relationships for the model system.

The solid−fluid potential in an infinite structureless single-walled cylindrical tube is given by[14]

$$U_{sf}(r,R) = \pi^2\rho_s\epsilon_{sf}\rho_{sf}^2\left\{\frac{63}{32}\left[\frac{R-r}{\sigma_{sf}}\left(1+\frac{r}{R}\right)^{-10}\right]F\left[-\frac{9}{2};-\frac{9}{2};1;\left(\frac{r}{R}\right)^2\right] - 3\left[\frac{R-r}{\sigma_{sf}}\left(1+\frac{r}{R}\right)^{-4}\right]F\left[-\frac{3}{2};-\frac{3}{2};1;\left(\frac{r}{R}\right)^2\right]\right\} \quad (1)$$

Here, r is the radial coordinate of the adsorbate molecule reckoned from the pore center, R denotes pore radii, ρ_s is the surface number density of carbon atoms, and $F[\alpha;\beta;\gamma;\delta]$ is the hypergeometric function. We must underline that the solid−fluid potential is of crucial importance in simulation studies of confinement fluid. As shown by Steele et al.,[26] Tanaka et al.,[27] and others, the potential given by eq 1 is a reasonable approximation of real solid−fluid interactions between adsorbed molecules and a structureless carbon tube. On the other hand, the solid−fluid interactions can be modeled by the other potentials that have been developed so far.[28] It is particularly important when the oxygen is add to the carbon nanotubes.[29]

The fluid−fluid interactions were computed from the truncated Lennard-Jones (LJ) pair potential,[30−32]

$$V_{ff}(r) = 4\epsilon_{ff}\left[\left(\frac{\sigma_{ff}}{r}\right)^{12} - \left(\frac{\sigma_{ff}}{r}\right)^{6}\right]\Theta(r_{cut} - r) \quad (2)$$

Here r is the distance between two interacting fluid molecules, σ_{ff} denotes LJ fluid−fluid collision diameter, ϵ_{ff} is the LJ fluid−fluid potential well depth, $r_{cut} = 5\sigma_{ff}$ is the cutoff distance, and Θ denotes the Heaviside function. No long-range corrections were applied. The fluid−fluid and solid−fluid parameters were chosen to mimic nitrogen in carbon pores at the nitrogen boiling temperature of 77 K. Well-defined and tested parameters were taken from the work of Ravikovitch et al.[33]

In the current work we used the Gauge Cell MC algorithm due to Neimark and Vishnyakov.[22,23] The simulation system consists of two cells: gauge and pore. The length of the pore cell (i.e., structureless single wall carbon tube) is equal to $10\sigma_{ff}$. Due to the cylindrical shape of the pore cell, the periodic boundary conditions were applied in the direction parallel to the pore wall. As a gauge cell, we employed a cube with triply periodic boundary conditions. The size of the gauge cell varied from $30\sigma_{ff}$ to $120\sigma_{ff}$ and was adjusted so that the sufficient number of fluid molecules (>30) were contained in the gauge cell during the simulation.[23] The gauge cell was calibrated by a series of Monte Carlo simulations in canonical ensemble with Widom's particle insertion method.[34] Similarly to the Gibbs Ensemble Monte Carlo Simulation due to Panagiotopoulos two types of Monte Carlo moves are performed: molecule displacement within the cells and molecule exchange between the cell.[31] In the displacement step the cells are independent and represent two unrelated canonical ensembles.[22] A molecule and cell were selected at random. Next, the position of the selected molecule was perturbed randomly to a new trial position. The displacement trial was accepted according to the standard Metropolis scheme,[35,22]

$$\min\{1, \exp(-\Delta E_\zeta/k_bT)\} \quad (3)$$

where the subscript ζ denotes selected cell (i.e., pore or gauge), ΔE_ζ is the configuration energy change in the selected cell, and k_bT is the thermal energy. The exchange step consists of an attempted molecule insertion in one of the cells coupled with attempted molecule deletion in the other cell. The position for the attempted molecule insertion and the molecule for the attempted deletion are chosen at random. A trial transfer from the gauge cell to the pore cell is accepted with a probability derived by Panagiotopoulos,[35,22]

$$\min\{1, \exp(-[\Delta E_p + \Delta E_g + k_bT\ln[V_g(N_p+1)/V_pN_g]]/k_bT)\} \quad (4)$$

where the subscript "p" denotes pore cell whereas subscript "g" denotes the gauge cell. Obviously, the same rule (with changed subscripts) is applied to a trial transfer from the pore cell to the gauge cell.

Each move (displacement in both pore and gauge cell, exchange molecule from pore to gauge cell, and in the reverse direction) has the same probability of occurrence. Such selection guarantees the microscopic reversibility since for exchange trial from pore to gauge cell and in the reverse direction, the probability was equal. To check the accuracy of the Gauge Cell MC we adopted two methods. The first one is checking whether the chemical potential was constant in the simulation system, i.e., in both pore and gauge cell by the Widom's particle insertion method.[34] The potential distribution theorem due to Widom is the standard method that works very well for not very dense inhomogeneous systems.[32] The second method was introduced in the current study. We constructed the simulation system consisting of two pore cells of equal radii but having different lengths and one standard gauge cell. Obviously, the displacement step was independent in three cells and accepted according to eq 3. The exchange step was constructed similarly to the standard Gauge Cell MC with additional exchange between the pore cells. Equation 4 was applied for both exchanges, i.e., between the gauge and selected pore cell and between the pore cells. As previously the probability of all steps was equal to 1 in 6 because the number of steps is increased to 6. During the Gauge Cell MC we measure the adsorbed density in pore cells independently. Obviously, at the thermodynamic equilibrium the density should be equal in both pore cells within statistical errors. Such an extended Gauge Cell MC seems to be a very promising tool for the investigation of fluid equilibrium in a series of pores of different pore radii.

The true equilibrium transition (i.e., phase coexistence) was determined by the thermodynamic integration along the generated continuous isotherm,[22,23]

$$\Omega(\mu,T) = \Omega(\mu_r,T) - \int_{\mu_r}^{\mu} N(\mu,T)\,d\mu = -k_bTN(\mu_r,T) - \int_{\mu_r}^{\mu} N(\mu,T)\,d\mu \quad (5)$$

where $\Omega(\mu,T)$ denotes the grand thermodynamic potential (volume V is fixed and does not appear as a variable in Ω), μ_r

is the chemical potential of the reference state (i.e., ideal gas), and $N(\mu,T)$ is the number of molecules directly calculated from the Gauge Cell MC.

The phase coexistence occurs when the grand thermodynamic potential of vaporlike and liquidlike states is equal:

$$\Omega_v(\mu_e,T) = \Omega_l(\mu_e,T) \tag{6}$$

Since we generated a full van der Waals loop consisting of stable, metastable, and unstable states, the vaporlike and liquidlike spinodal can be directly determined from Gauge Cell MC results. In a series of papers Neimark et al.[22,23,36] showed that the Gauge Cell MC combined with eq 5 is in agreement with thermodynamic integration developed by Peterson and Gubbins. For this reason we paid attention to the Gauge Cell MC according to Neimark and Vishnyakov.[22,23]

2.2. Improved Derjaguin−Broekhoff−deBoer (IDBdB) Theory. In the previous section we described the Gauge Cell MC implemented with thermodynamic integration, which can be used for the evaluation of the relationship between the condensation/evaporation pressures versus pore size. Unfortunately, the generation of the whole van der Waals loop is not effective for large pore size due to two facts. At first, increasing pore size causes a drastic increase in Gauge Cell MC time since the number of molecules is relatively large. Next, the well-developed van der Waals loop starts to deform when the pore size increases due to the inhomogeneous state of the fluid in the pore, i.e., formation of bubbles and bridges.[37] So it is reasonable to apply the phenomenological thermodynamic approach for generating the relationships mentioned above. Beside this, we should take into consideration the fact that for the calculation of pore size distribution we need to know the analytical relationship between the condensation/evaporation pressures and the pore size of the introduced simplified model. Clearly, both approaches should overlap over the whole range of internal cylindrical tube pore radii. For these reasons we applied the concept of the IDBdB method.[6]

The details of the IDBdB theory were described elsewhere.[6] As shown by Kowalczyk et al.[6] the predictions of the capillary condensation/evaporation curves in the MCM-41 silica cylindrical tubes are in close agreement with the empirical relationship due to Kruk−Jaroniec−Sayari (KJS) as well as with the Non-local Density Functional Theory (NDFT) according to Ravikovitch−Neimark treatment. Moreover, the prediction of the average pore size of these highly ordered well-defined silica materials by IDBdB theory was in close agreement with the XRD measurements.

The first step toward the implementation of the IDBdB theory is the calibration of the disjoining pressure isotherm on carbon using the isotherm for silica. Note that the interaction of nitrogen molecules with graphite surface is stronger than that with silica. For this reason in the current proposition we keep the form of the disjoining pressure isotherm whereas the parameters were calibrated to M32B carbon black surface,[39]

$$\Pi_1 \exp(-h/\lambda_1) + \Pi_2 \exp(-h/\lambda_2) = -(RT/v_m)\ln(p/p_0) \tag{7}$$

Here Π_1 and Π_2 characterize the strength of the surface forces field and the parameters λ_1 and λ_2 are the decay length in the order of a monolayer thickness (i.e. λ_1,λ_2 characterize the range of structural forces action), R is the universal gas constant, T is the temperature, ν_m is the molar liquid density of an adsorbate, and p/p_0 is the relative pressure of an adsorbate. We investigated several commercial carbon black surfaces to calibrate the parameters of the disjoining pressure isotherm given by eq 7.

TABLE 1: Parameters for the Disjoining Pressure Isotherm of Nitrogen at 77 K Adsorbed on the Reference M32B Carbon Flat Surface

parameter	M32 carbon black
Π_1, MPa	68.03339
Π_2, MPa	578.27071
λ_1, nm	3.51888
λ_2, nm	1.06898

We got the best agreement with the Gauge Cell MC results using M32B carbon black.

According to the IDBdB method the relationship between both critical film thickness and critical capillary radius, as a function of the relative pressure for the open-ended cylindrical capillary is given by,[6]

$$\begin{cases} \dfrac{\gamma_\infty(r-h-2\delta)}{(r-h)^3} - \dfrac{\Pi_1}{\lambda_1}\exp(-h/\lambda_1) - \dfrac{\Pi_2}{\lambda_2}\exp(-h/\lambda_2) = 0 \\ \dfrac{\gamma_\infty(r-h-\delta)}{(r-h)^2} + \Pi_1\exp(-h/\lambda_1) + \Pi_2\exp(-h/\lambda_2) = \\ \qquad -(RT/v_m)\ln(p/p_0) \end{cases} \tag{8}$$

where γ_∞ denotes surface tension for the bulk fluid, and δ is the displacement of the surface of zero mass density relative to the surface of tension. The physical meaning of δ and its impact on the spinodal condensation point were presented previously.[6]

The IDBdB method gives the relationship for the direct estimation of the equilibrium transition in considered geometry. It can be written as follows:[6]

$$\begin{cases} \ln(p/p_0) = [\Pi_1\exp(-h_e/\lambda_1) + \Pi_2\exp(-h_e/\lambda_2)]\dfrac{\nu_m}{RT} + \dfrac{\gamma_\infty\nu_m\left(1-\dfrac{\delta}{r-h_e}\right)}{RT(r-h_e)} \\ \ln(p/p_0) = \dfrac{2\dfrac{\gamma_\infty\left(1-2\dfrac{\delta}{r-h_e}\right)}{RT} + 2\dfrac{\nu_m}{RT(r-h_e)}[\zeta_1+\zeta_2]}{r-h_e} \end{cases} \tag{9}$$

where the coefficients ζ_1 and ζ_2 are given by[6]

$$\zeta_1 = \Pi_1\lambda_1\{\exp(-h_e/\lambda_1)[r-\lambda_1-h_e] + \lambda_1\exp(-r/\lambda_1)\} \tag{10}$$

$$\zeta_2 = \Pi_2\lambda_2\{\exp(-h_e/\lambda_2)[r-\lambda_2-h_e] + \lambda_2\exp(-r/\lambda_2)\} \tag{11}$$

As one can see the formulas given by eqs 8 and 9 are the classical Kelvin equations corrected for the surface forces and varying surface tension according to the Gibbs−Tolman−Koenig−Buff proposal. For larger pore radii the equations reduce to the DBdB theory developed by Ravikovitch and Neimark since $\gamma(r_m) \rightarrow \gamma_\infty$.[40] Finally, for the sufficiently large value of the pore radii the disjoining pressure isotherm terms can be neglected and the classical Kelvin relationships are equivalent with eqs 8 and 9. The main difficulty in the proper estimation of both spinodal condensation and equilibrium transition in the cylindrical capillary corresponds to the boundary of the micro- and mesoporosity (i.e., pore radii of interest $R \approx 1-3$ nm). As we mentioned above, the IDBdB method was

verified previously on a series of regular MCM-41 silica materials. For this reason in the current paper we also use it. Also it should be noted that a similar approach was introduced by Dubinin et al.,[41] but has not received attention in the scientific community.

2.3. Internal Pore Size Distribution of SWNHs. As we mentioned above, the model of SWNHs can be simplified to an infinitely long carbon single-wall cylindrical capillary due to small adsorption in a cone.[18] Such a model seems to be a realistic one if we take into account that the simplified SWNH is a well-defined crystalline single-wall carbon graphite rolled into tube. Moreover, some researchers investigated the properties of the capillary condensation/evaporation of nitrogen at 77 K in carbon tubes by simulation in the Grand Canonical Ensemble. As a result, the simulation system has been well-defined and tested previously. Our simplification is also justified by the fact that we are interested in thermodynamics properties (i.e., excess Gibbs of adsorption, absolute value of adsorption, isosteric heat of adsorption) and not in dynamic quantities. It is obvious that the dynamic quantities (i.e., diffusion coefficient, an so on) can be sensitive to the atomics structure of the carbon tube and the presence of a cone.

The key problem is the estimation of the pore size distribution of SWNHs from the single nitrogen adsorption isotherm measured at 77 K. As we mentioned above, we can obtain the isotherm in the internal space of the SWNHs by simple measurements. Such a single nitrogen isotherm can be used for the estimation of the distribution of pore sizes by applying the general concept of the integral equation[20,42,43] or modified iterative algorithm due to Dollimore and Heal.[21]

According to the integral theory of adsorption the experimental adsorption isotherm normalized to unity, $\theta_{tot}(\xi)$, is modeled as a superposition of adsorption isotherms in pores of different sizes[2−4]

$$\theta_{tot}(\xi) = \int_{R_{min}}^{R_{max}} \theta_{loc}(\xi,R) f(R)\, dR, \quad \xi \in [a,b] \qquad (12)$$

where $\xi = p/p_0$ denotes relative pressure, R_{min} is the minimal pore size (molecule diameter), R_{max} is the largest pore size, and $f(R)$ is the normalized and positive defined distribution function giving pore size distribution. The kernel of the integral equation defined by eq 12 can be obtained from IDBdB method[44]

$$\theta_{loc}(\xi,R) = \begin{cases} h(\xi,R)/h_{cr}(R), & h(\xi,R) < h_{cr}(R) \\ 1, & \text{elsewhere} \end{cases} \qquad (13)$$

here $h(\xi,R)$ denotes the thickness of the adsorbed film, and $h_{cr}(R)$ is the film thickness at the vaporlike spinodal. In eq 13 we assume that for proper estimation of $f(R)$ the vaporlike spinodal (i.e., adsorption branch of the experimental hysteresis loop) can be used. This assumption is justified by three arguments. At first, the experimental nitrogen isotherm on SWNHs at 77 K is reversible (see Figure 7). Next, in the series of recent studies of structural heterogeneity of well-defined regular silica materials the authors recommended the adsorption branch of the experimental hysteresis loop for the pore size analysis.[5,6,45] Finally, the adsorption branch of the experimental hysteresis loop is not disturbed by the connectivity effect.[46]

The second method frequently used for the estimation of the pore size distribution of porous materials from a single adsorption isotherm is an iterative algorithm due to Dollimore and Heal (DH).[21] Unfortunately, the original DH approach cannot be used for cylindrical capillaries of small pore radii due to limitations of the Kelvin equation. For this reason we modified the DH algorithm. A detailed description of the DH algorithm as well as the modification is given elsewhere.[21,44]

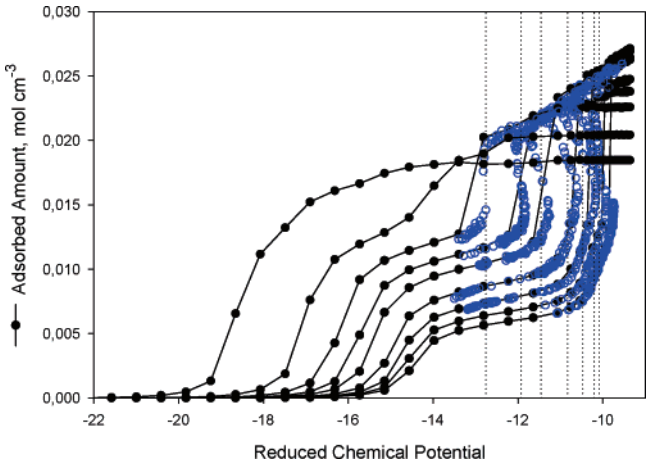

Figure 2. Full GCMC (black circles) and Gauge Cell MC (blue circles) adsorption isotherms of nitrogen at 77 K for structureless single-walled carbon tubes of reduced radii: 2, 2.5, 3, 3.5, 4, 5, 6, 7, and 8. Dotted vertical lines show the location of vapor−liquid coexistence in the pore determined from the thermodynamic integration (i.e., Maxwell rule of equal areas). Inside the carbon nanotube the unstable states on the van der Waals loop are being stabilized by the proper choice of the volume of the gauge cell coupled to the tube. Both pressure and chemical potential of nitrogen are equal in the pore and gauge cell.

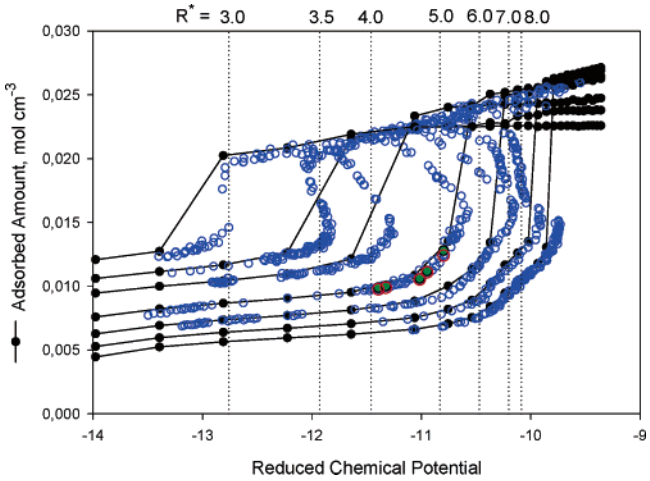

Figure 3. GCMC (black circles) and Gauge Cell MC (blue circles) adsorption isotherms of nitrogen at 77 K for structureless single-walled carbon tubes. The open red and closed red circles are selected at the adsorption points obtained in the extended Gauge Cell MC (i.e., simulation system consists of two pore and one gauge cell). Dotted vertical lines show the location of vapor−liquid coexistence in the pore determined from the thermodynamic integration (i.e., Maxwell rule of equal areas). Inside the carbon nanotube the unstable states on the van der Waals loop are being stabilized by the proper choice of the volume of the gauge cell coupled to the tube. Both pressure and chemical potential of nitrogen are equal in the pore and gauge cell.

3. Results and Discussion

The final results obtained form Gauge Cell MC supported with thermodynamic integration are displayed in Figures 2−6. Figures 2 and 3 report a full van der Waals loop consisting of stable, metastable, and unstable states and an equilibrium coexistence point calculated by the thermodynamic integration along the continuous isotherm. Additionally, for checking the accuracy of the Gauge Cell MC the adsorption isotherms calculated from the standard GCMC are attached. It is worth nothing that the states generated in GCMC and in the Gauge

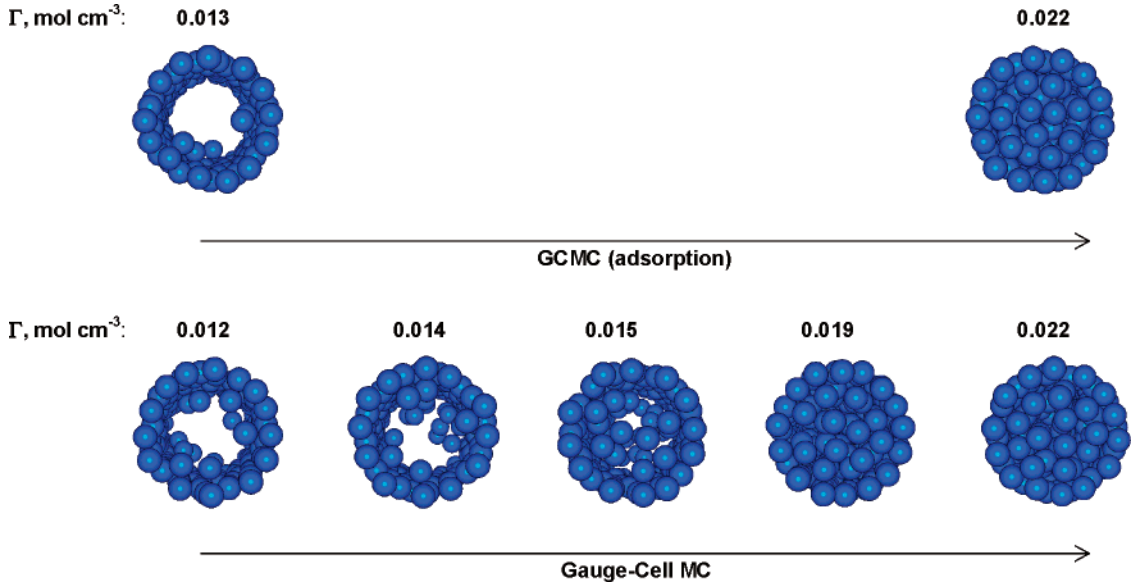

Figure 4. Snapshots of nitrogen at 77 K in the structureless single-walled carbon nanotube of $R^* = 3$ at various adsorbed densities. The states with adsorbed density $\Gamma = 0.014$, 0.015, 0.019 were stabilized in the Gauge Cell MC, whereas the first-order phase transition form vaporlike to liquidlike fluid structure was obtained in a standard GCMC scheme.

Cell MC overlap with remarkable accuracy. For the reduced pore radius $R^* \equiv R\sigma_{ff}^{-1} = 3$ (σ_{ff} denotes the Lennard-Jones collision diameter of nitrogen) we observe in the Gauge Cell MC a sharp transition between vaporlike and liquidlike states of fluid in the considered carbon cylindrical pore. The spinodals of the van der Waals loop coincide. We can argue that below $R^* = 3$ the adsorption−desorption isotherm is fully reversible (i.e., supercritical in nature). GCMC results confirm this observation (see Figure 2). Increasing the pore size causes development of the symmetrical well-defined van der Waals loops and the equilibrium transition corresponds to the Maxwell rule of equal areas. For the largest pores of $R^* = 7$ or 8 we observe the deformation of the van der Waals loops due to the formation of thin bridges. According to the extensive investigations due to Vishnyakov and Neimark[37] the equilibrium transition obtained for the short pore cell (i.e., $L^* = 10$) agrees with the one generated in the long pore cell (i.e., $L^* = 30$). This observation validates the present calculations. Similarly to Neimark et al.[22,23] we observe the largest disagreement between the vaporlike spinodal point calculated from the GCMC and the Gauge Cell MC for the smallest pore radii. Obviously, we can reduce the disagreement between these two methods by increasing the grid in the chemical potential used as an input in the GCMC. Note that due to statistical errors the oscillations on the van der Waals loops are recognized. The true spinodals were calculated from the Gauge Cell MC according to the simple parabolic interpolation method described by Neimark et al.[22] In Figure 4 we display the detailed structure of the equilibrium states obtained form the GCMC and the Gauge Cell MC for arbitrarily selected reduced pore radius ($R^* = 3$). Due to the lack of certain constraints on the density fluctuations in the GCMC, the spontaneous condensation occurs below the true vaporlike spinodal calculated from the Gauge Cell MC. The metastables and unstable states of the fluid in the structureless carbon cylindrical pore between spinodals can be observed only in the Gauge Cell MC. The selective results obtained from the extended Gauge Cell MC are displayed in Figures 3 and 5. As one can notice the adsorbed density in two pore cells is the same, within statistical error, at the thermodynamic equilibrium. Clearly, these results overlap with those obtained from the original Gauge Cell MC (see Figure 3). This fact justifies the

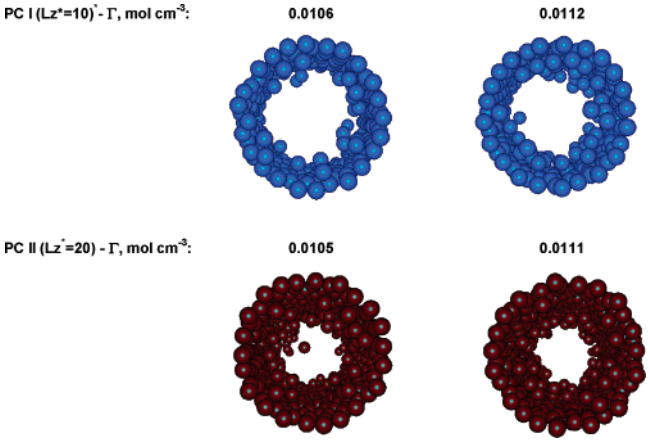

Figure 5. Snapshots of nitrogen at 77 K in the two structureless single-walled carbon nanotubes of the same radius $R^* = 5$ at two arbitrarily selected adsorbed densities. The extended Gauge Cell MC consists of two pore cells of different reduced length: 10 and 20. At equilibrium the adsorbed density was equal within statistical errors.

present calculations and gives the possibility of extending the Gauge Cell MC for the investigation of the inhomogeneous fluids in the series of connected cylindrical pores characterized by different sizes. The dependences of the spinodals and equilibrium transition upon pore size calculated from Gauge Cell MC are displayed in Figure 6. Spontaneous evaporation occurs at lower pressure (or chemical potential) than that observed for spontaneous condensation. The correlation between the Gauge Cell MC results and the IDBdB predictions is very good; however, the reversibility of the adsorption−desorption isotherm is not achieved by the IDBdB method (see Figure 6). The equilibrium transition and vaporlike spinodal computed from the IDBdB approach correspond to that obtained from the Gauge Cell MC. The pressure for the liquidlike spinodal is the smallest one. The prediction of the classical DBdB method cannot be used for the estimation of the distribution of sizes of the SWNHs due to the large deviation from the Gauge Cell MC predictions.

The experimental data on closed and open SWNHs are presented in Figure 7. Using cubic splines the adsorption

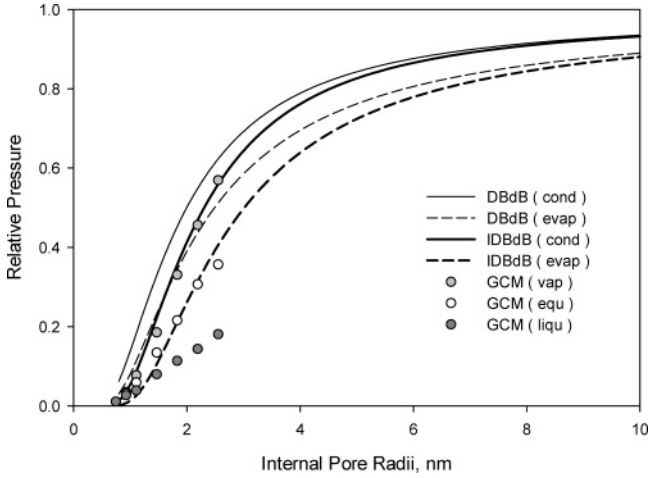

Figure 6. Comparison of the results obtained from Gauge Cell MC (vap = vaporlike spinodal, equ = equilibrium transition, liqu = liquidlike spinodal) with capillary condensation (solid lines)/evaporation (dotted lines) curves computed from the classical DBdB method (thin lines) and the improved DBdB method (bold lines).

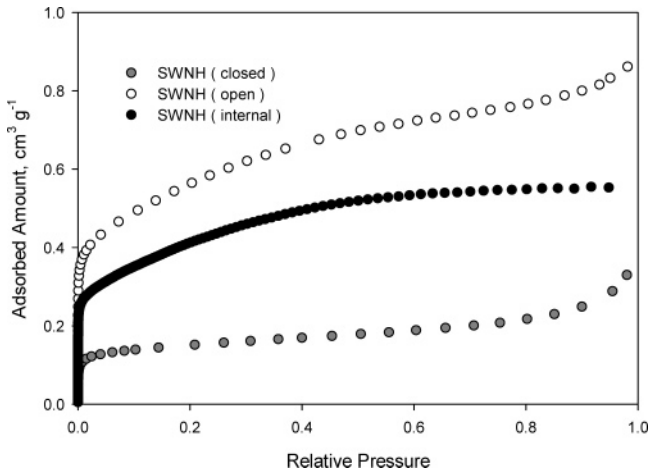

Figure 7. Nitrogen adsorption isotherms at 77 K for closed SWNH (gray circles), open SWNH (white circles), and the internal space of SWNH (black circles).

isotherm in the internal space of SWNHs is calculated and also displayed in Figure 7. What is more interesting, the adsorption isotherm in the internal space of SWNHs is characterized by the gradual increase, with a plateau at $p/p_0 \cong 0.5$, suggesting a relatively broad pore size distribution. The importance of the conical cap in the adsorption of the low-pressure region is a well-known fact. At low pressures the enthalpy of adsorption is the highest because the high energetic centers are filled by adsorbed molecules gradually. Since the curvature effect of the conical cap is very high we suspect that in the Henry region the adsorption is dominated by the filling of the interstitial spaces between conical caps of neighboring SWNHs. The cylindrical parts of SWNHs are filled at a higher relative pressure, approximately $p/p_0 > 0.1$. For this reason, we describe the experimental adsorption isotherm in the range of relative pressure excess the assumed $p/p_0 > 0.1$. A similar procedure was adopted by Ravikovitch et al.[47] and Kowalczyk et al.[6] We believe that this simplification is not critical for the current method; however, for the proper description of the nitrogen adsorption isotherm at 77 K in the whole range of the relative pressure the conical section should be included in the model. The theoretical description of the adsorption isotherm in the internal space of SWNH given by eq 13 agrees extremely well

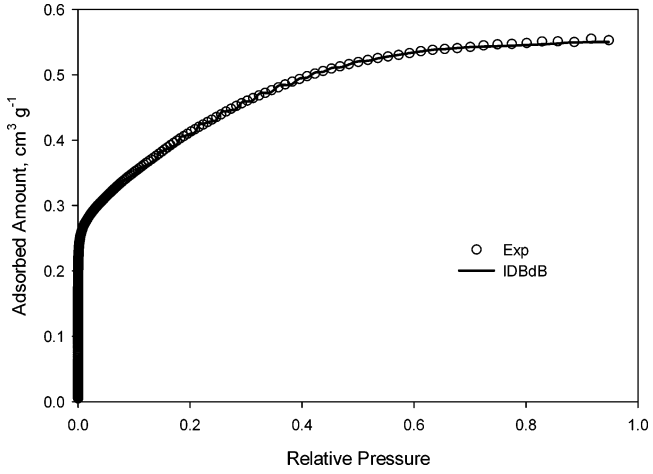

Figure 8. Fitting of the nitrogen experimental adsorption isotherm at 77 K on the internal space of SWNH (open circles) by the IDBdB method (solid line).

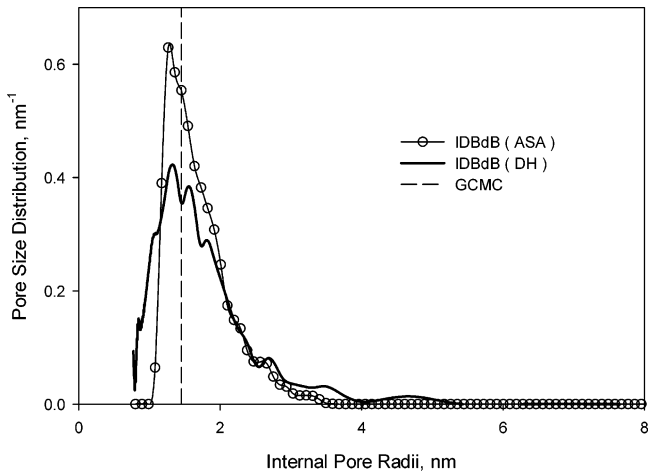

Figure 9. Pore size distribution of the internal space of SWNH calculated from the IDBdB method by inverting the adsorption integral equation (ASA) and the modified DH algorithm (DH). The vertical dashed line shows the prediction of the average pore size calculated from GCMC by Ohba et al.[42]

with experiment (see Figure 8). Please note the excellent agreement between the theory and experiment.

The main result for this analysis is shown in Figure 9. Here, we presented pore size distributions calculated from both integral theory of adsorption and the modified DH method. The average internal pore radii calculated from both methods are equal to 1.69 and 1.78 nm, whereas the standard deviations are equal to 0.24 and 0.39 nm, respectively. According to Ohba et al. the average pore size is equal to 1.45 nm. Bearing in mind the simplified model used by Ohba et al.[48] (i.e., the assumption that the distribution function is a delta Dirac one) the agreement is satisfactorily. Our results are the following: the distribution of the cylindrical pore radii of the SWNHs assembly is relatively large in comparison to that of the novel ordered silica-type materials. The internal pore radii varied in the range 1.0−3.6 nm with the maximum at 1.3 nm. The computed distribution of sizes of SWNHs can be used to interpret the data for the adsorption, transport, electronic conduction, and other properties.

Acknowledgment. The authors thank to Professor A. V. Neimark (TRI, Princeton, U.S.A.) and Dr. A. P. Terzyk (Nicolaus Copernicus University, Torun, Poland) for fruitful comments connected with the current study. P.K. thanks Professor A. Z. Panagiotopoulos (Department of Chemical

Engineering, Princeton University, U.S.A.) for sending the papers connected with Gibbs Ensemble simulation and fruitful comments.

References and Notes

(1) Gregg, S. J.; Sing, K. S. W. *Adsorption, Surface Area and Porosity*; Academic Press: London, UK, 1982.
(2) Jaroniec, M.; Madey, R. *Physical Adsorption on Heterogeneous Solids*; Elsevier: Amsterdam, The Netherlands, 1988.
(3) Do, D. D. *Adsorption Analysis*: *Equilibria and Kinetics*; Imperial College Press: London, UK, 1998.
(4) Rudzinski, W.; Everett, D. H. *Adsorption of Gases on Heterogeneous Surfaces*; Academic Press: New York, 1992.
(5) Kruk, M.; Jaroniec, M.; Sayari, A. *Langmuir* **1997**, *13*, 6267.
(6) Kowalczyk, P.; Jaroniec, M.; Terzyk, A. P.; Kaneko, K.; Do, D. D. *Langmuir* **2005**, *21*, 1827.
(7) Kruk, M.; Jaroniec, M. *Chem. Mater.* **2001**, *13*, 3169.
(8) Pikunic, J.; Clinard, C.; Cohaut, N.; Gubbins, K. E.; Guet, J. M.; Pellenq, R. J. M.; Rannou, I.; Rouzaud, J. N. *Langmuir* **2003**, *19*, 8565.
(9) Iijima, S. *Nature* **1991**, *354*, 56.
(10) Endo, M.; Muramatsu, H.; Hayashi, T.; Kim, Y. A.; Terrones, M.; Dresselhaus, M. S. *Nature* **2005**, *433*, 476.
(11) Murata, K.; Kaneko, K. *Chem. Phys. Lett.* **2000**, *321*, 342.
(12) Miyawaki, J.; Yudasaka, M.; Iijima, S. *J. Phys. Chem. B* **2004**, *108*, 10732.
(13) Ajayan, P. M.; Iijima, S. *Nature* **1993**, *361*, 333.
(14) Tanaka, H.; El-Merraoui, M.; Steel, W. A.; Kaneko, K. *Chem. Phys. Lett.* **2002**, *352*, 334.
(15) Iijima, S.; Yudasaka, M.; Yamada, R.; Bandow, S.; Suenaga, K.; Kokai, F.; Takahashi, K. *Chem. Phys. Lett.* **1999**, *309*, 165.
(16) Bekyarova, E.; Kaneko, K.; Yudasaka, M.; Kasuya, D.; Iijima, S.; Huidobro, A.; Rodriguez-Reinoso, F. *J. Phys. Chem. B* **2003**, *107*, 4479.
(17) Murata, K.; Kaneko, K.; Steele, W. A.; Kokai, F.; Takahashi, K.; Kasuya, D.; Hirahara, K.; Yudasaka, M.; Iijima, S. *J. Phys. Chem. B* **2001**, *105*, 10210.
(18) Tanaka, H.; Kanoh, H.; El-Merraoui, M.; Steele, W. A.; Yudasaka, M.; Iijima, S.; Kaneko, K. *J. Phys. Chem. B* **2004**, *108*, 17457.
(19) Bekyarova, E.; Hashimoto, A.; Yudasaka, M.; Hattori, Y.; Murata, K.; Kanoh, H.; Kasuya, D.; Iijima, S.; Kaneko, K. *J. Phys. Chem. B* **2005**, *109*, 3711.
(20) Kowalczyk, P.; Terzyk, A. P.; Gauden, P. A. *Langmuir* **2002**, *18*, 5406.
(21) Dollimore, D.; Heal, G. R. *J. Appl. Chem.* **1964**, *14*, 109.
(22) Neimark, A. V.; Vishnyakov, A. *Phys. Rev. E* **2000**, *62*, 4611.
(23) Vishnyakov, A.; Neimark, A. V. *J. Phys. Chem. B* **2001**, *105*, 7009.
(24) Ravikovitch, P. I.; Neimark, A. V. *Stud. Surf. Sci. Catal.* **2000**, *129*, 597.
(25) Neimark, A. V.; Ravikovitch, P. I.; Vishnyakov, A. *J. Phys. Condens. Matter* **2003**, *15*, 47.
(26) Steele, W. A.; Bojan, M. J. *Adv. Colloid Interface Sci.* **1998**, *76*−*77*, 153.
(27) Tanaka, H.; Kanoh, H.; Yudasaka, M.; Iijima, S.; Kaneko, K. *J. Am. Chem. Soc.* **2005**, *127*, 7511.
(28) Beran, S.; Dubsky, J.; Slanina, Z. *Surf. Sci.* **1979**, *79*, 39.
(29) Slanina, Z.; Stobinski, L.; Tomasik, P.; Lin, H. M.; Adamowicze, L. *J. Nanosci. Nanotechnol.* **2003**, *3*, 193.
(30) Do, D. D.; Do, H. D.; Ustinov, E. A. *Langmuir* **2003**, *19*, 2215.
(31) Allen, M. P.; Tildesley, D. J. *Computer Simulation of Liquids*; Clarendon Press: Oxford, UK, 1987.
(32) Frenkel, D.; Smit, B. *Understanding Molecular Simulation*: *From Algorithms to Applications*; Academic Press: New York, 1996.
(33) Ravikovitch, P. I.; Vishnyakov, A.; Neimark, A. V. *Phys. Rev. E* **2001**, *64*, 011602.
(34) Widom, B. *J. Chem. Phys.* **1963**, *39*, 2808.
(35) Panagiotopoulos, A. Z. *Mol. Phys.* **1987**, *62*, 701.
(36) Neimark, A. V.; Ravikovitch, P. I.; Vishnyakov, A. *Phys. Rev. E* **2002**, *65*, 031505.
(37) Vishnyakov, A.; Neimark, A. V. *J. Chem. Phys.* **2003**, *119*, 9755.
(38) Tolman, R. C. *J. Chem. Phys.* **1949**, *17*, 119.
(39) Kowalczyk, P.; Tanaka, H.; Kanoh, H.; Kaneko, K. *Langmuir* **2004**, *20*, 2324.
(40) Neimark, A. V.; Ravikovitch, P. I. *Microporous Mesoporous Mater.* **2001**, *44*−*45*, 697.
(41) Dubinin, M. M.; Kataeva, L. I.; Ulin, V. I. *Bull. Akad. Nauk SSSR, Ser. Khim.* **1981**, *30*, 25.
(42) Gauden, P. A.; Kowalczyk, P.; Terzyk, A. P. *Langmuir* **2002**, *19*, 4253.
(43) Morozov, V. A. *Methods for Solving Incorrectly Posed Problems*; Springer: Berlin, Germany, 1984.
(44) Kowalczyk, P.; Gun'ko, V. M.; Terzyk, A. P.; Gauden, P. A.; Rong, H.; Ryu, Z.; Do, D. D. *Appl. Surf. Sci.* **2003**, *206*, 67.
(45) Ustinov, E. A.; Do, D. D.; Jaroniec, M. *J. Phys. Chem. B* **2005**, *109*, 1947.
(46) Kruk, M.; Celer, E. B.; Jaroniec, M. *Chem. Mater.* **2004**, *16*, 698.
(47) Ravikovitch, P. I.; Neimark, A. V. *Langmuir* **2002**, *18*, 1550.
(48) Ohba, T.; Murata, K.; Kaneko, K.; Steele, W.; Kokai, F.; Takahashi, K.; Kasuya, D.; Yudasaka, M.; Iijima, S. *Nano lett.* **2001**, *1*, 371.